Three-Pulse Photon Echo Measurements on the Accessory Pigments in the Reaction Center of *Rhodobacter sphaeroides*

Marie-Louise Groot, Jae-Young Yu, Ritesh Agarwal, James R. Norris, and Graham R. Fleming*,†

Department of Chemistry and the James Franck Research Institute, The University of Chicago, Chicago, Illinois 60637

Received: January 23, 1998; In Final Form: April 24, 1998

Frequency-resolved, three-pulse photon echo peak shifts of the accessory pigments of the reaction center of *Rhodobacter sphaeroides* were recorded to study the ultrafast pigment−protein dynamics. For a qualitative understanding of the data, which includes an increase in rephasing capability after 1 ps, it is necessary to take into account the influence of the primary electron donor P on the 800 nm absorption band and direct electron transfer from the excited accessory bacteriochlorohyll B_A. The peak shift data and the absorption spectrum are simulated via the time correlation function of the optical transition frequency. We observe subtle differences in the dynamics on the blue and red side of the absorption band, which may be related to differences in the environment between the B_A and B_B pigments, respectively. The bath correlation time is longer, ∼90 fs, at 810 nm than at 790 nm, where it is ∼60 fs. Since we conclude from our transient grating measurements that the time of energy transfer is 80 fs at 810 nm and 130 fs at 790 nm, this indicates that around 810 nm no significant nuclear relaxation takes place prior to energy transfer. On a longer time scale we observe coherent oscillations of low frequency, ∼3−4 and 36 cm^{-1}, and a small ∼30 ps decay of rephasing capability.

Introduction

One of the key reactions in photosynthesis is the conversion of excitation energy into a charge-separated state. This occurs in a membrane bound pigment−protein complex, called the reaction center, where following electronic excitation an electron is transferred in successive steps from one side of the membrane to the other.[1−3]

A well-studied reaction center is that of the purple bacterium *Rb. sphaeroides*, which consists of 4 bacteriochlorophyls (Bchl), 2 bacteriopheophytins (H), and 2 quinone molecules arranged in a protein scaffold in a pseudo-C_2 symmetry.[4,5] The primary electron donor, P, is formed by a pair of closely interacting Bchls. Despite the symmetric arrangement of the pigments in two branches, electron transfer occurs only along the pigments on the A branch. Upon excitation of P, an electron is transferred to the bacteriopheophytin H_A in ∼3 ps. Two accessory Bchl molecules, B_A and B_B, are located between the primary donor and the H_A and H_B pigments, respectively. The role of B_A in the electron-transfer process, whether it is a real or a virtual intermediate, has been the subject of much debate. This debate was caused because it proved difficult to observe spectral changes related to the state $P^+B_A^-$. With the observation of such spectral transients by several groups, there now seems to be consensus that charge separation occurs from P to B_A in ∼3 ps and from B_A to H_A in ∼1 ps.[6−12] Subsequent electron transfer from H_A to the secondary quinone acceptor Q_A is much slower and occurs in ∼200 ps.

The B and H pigments are also active in ultrafast[13,14] downward (see absorption spectrum in Figure 1) energy transfer to P. The energy transfer from B to P takes about 100−120 fs,[15−19] which was determined from experiments in which either the recovery of the absorption of the B pigments was measured or the bleaching and stimulated emission from the lower exciton level of P, P_-, appeared upon excitation at 800 nm. This rate is faster than predicted by Förster (dipole−dipole coupling) theory in the very weak limit, and also the observed weak temperature dependence cannot be explained by this type of transfer.[18] The energy transfer from B to P has therefore been suggested[17] to occur via the upper exciton level of P (∼815−825 nm) in the strong coupling limit of Förster theory or by direct orbital overlap, i.e., via electron exchange interactions, between B and P.[17,18,20,21]

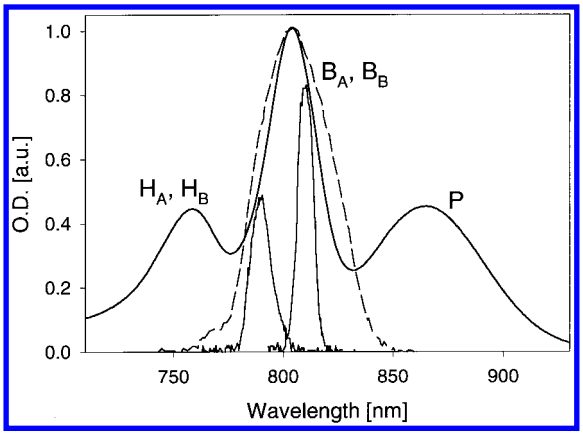

Figure 1. Reaction center absorption spectrum (solid line), laser spectrum (dashed line), and the spectral detection window of the filters, i.e., laser spectrum measured after the interference filters (solid lines). The filters peak at 790 nm with a fwhm of 176 cm^{-1} and at 810 nm with a fwhm of 126 cm^{-1}.

Recent experiments have yielded results that challenge the classical picture outlined above, in which H and B transfer their energy on an ultrafast time scale to the primary donor P. Several

† Permanent address: Department of Chemistry, University of California, Berkeley, Berkeley, CA 94720. E-mail: fleming@cchem.berkeley.edu.

S1089-5647(98)00868-2 CCC: $15.00
Published on Web 07/01/1998

groups[22−24] concluded that upon excitation of H and B direct formation of radical pairs, i.e., P^+B^- or B^+H^-, without the involvement of P*, competes with energy transfer from these pigments. The work of ref 25 showed that this occurs mainly on the blue side of the 800 nm band and therefore involves the accessory pigment on the active branch, B_A. These radical pair states must consequently be strongly coupled to the optically excited B_A* and H_A* states. Another issue related to this is whether the accessory bacteriochlorophylls and bacteriopheophytins should be considered as monomeric or whether the electronic coupling is strong enough to consider the pigments in the RC as a supermolecule.[26−32] This issue is still unresolved, at least in part because a correct description depends on the relaxation processes that occur and therefore on the time scale of the experiments.[22] For a more quantitative discussion on this subject, parameters such as the coupling strength to the bath (protein) and the time scale of the bath dynamics in relation to the electronic coupling strength and the energy-transfer times are required.

We have performed three-pulse stimulated photon echo experiments on the accessory B pigments. The three-pulse photon echo technique may be viewed as complementary to time-resolved absorption difference or fluorescence spectroscopy since it measures not the population decay but the decay of rephasing capability of the electronic state. The peak shift of the echo from zero is directly related to the time-correlation function of the optical transition,[33] and information such as the homogeneous line width and the optical dephasing time as well as fluctuations of the optical transition can be obtained from it.[34,35] So far as photosynthetic complexes are concerned, the three-pulse photon echo technique has been applied to the LH1 and LH2 antenna complexes[36] and the B820 subunit[37] to study the exciton delocalization length and the nature of the energy-transfer hopping process. Recently it was applied also to light harvesting systems obtained from the phycobilisomes of cyanobacteria.[38]

Material and Methods

Detergent isolated reaction centers of Rb. *sphaeroides*[39] were diluted to an OD of 0.2 at 800 nm in a cell with 0.2 mm path length. Sodium ascorbate (300 mM) was added to prereduce Q_A in order to prevent accumulation of the long-lived $P^+Q_A^-$ state. The sample was flowed with a peristaltic pump and chilled with ice water. The experiments were performed with a mode-locked Ti:sapphire laser with intracavity razor blades to shape the spectrum of the pulses. This produced pulses of 25−28 fs fwhm with a spectral width of 630 cm^{-1} centered around 800 nm (see Figure 1). The total pulse energy incident on the sample was varied between 1.5 and 4 nJ (no effect was observed), at a repetition rate of 250 kHz. The beams were focused in the sample with a 20 cm focal length achromatic lens.

The three-pulse echo peak shift technique as used here has been described in detail in ref 34. Briefly, the laser beam is split into three equal parts and collected on the focusing lens in a triangle configuration. Two of the beams travel over variable delay lines with which the coherence period (time delay between the first and second pulse) and the population period (time delay between the second and third pulse) are controlled. The interaction of the sample with the first pulse creates a coherent state, the second pulse puts the system in a population state, either the ground or excited state, and the third pulse again creates a coherent state. If the phase in each of the coherence periods is opposite, rephasing will occur, and an echo *E* field emerges from the sample after a certain delay time. We measured the integrated intensity of the echo signal in both phase-matched directions $k = k_3 \pm (k_1 - k_2)$ as a function of the coherence time. An experiment consists of measuring the echo profiles as a function of the population time *T*.

The echo peak shift from zero as a function of the population time is related to the time correlation function of the electronic transition frequency, $M(t)$.[33] Data analysis consists therefore of constructing a correlation function $M(t)$ that is capable of reproducing both the peak shift curve and the experimental absorption spectrum.[34,35] In short, this procedure consists of constructing $M(t)$, from which the line broadening function $g(t)$ is calculated. The eight nonlinear response functions that determine the echo peak shift are calculated from both the real and the imaginairy part of $g(t)$. In the simulations the actual pulse width is taken into account. The absorption spectrum is given by

$$\int_{-\infty}^{\infty} \mathrm{d}t \exp[-i(\omega - \omega_{eg})t] \exp[-g(t)]$$

We have also measured the echo peak shift on the blue and red side of the 800 nm band, by placing 790 and 810 nm interference filters (bandwidth 10 nm) after the sample; see Figure 1 for the resulting spectral detection window. We argue that by performing the post-sample frequency selection, the frequency grating in the sample is not interfered with. If the sample is heterogeneous, the rephasing capability may be different on the red and the blue side of the absorption band. By spectrally separating the echo signal, we can distinguish the rephasing capability within the absorption band. To check whether the post-sample frequency selection gives different results as opposed to pre-sample frequency selection (i.e., tuning the laser pulses at 785 and 810 nm), we measured the peak shift of the laser dye IR144 in methanol. We found no difference in time scales in the peak shift in the post- and pre-sample frequency selection.

Results

Transient Grating Data. When the delay between the first two pulses is set to zero, the pulses interfere in the sample and create a spatial population grating. The intensity of the scattering of the third pulse off the grating in the phase matched directions, $k = k_3 \pm (k_1 - k_2)$, measures the lifetime of the grating. In this case the grating will be destroyed by population decay since the spatial modulation is too large for the grating to decay by spatial diffusion.

The transient grating signal in Figure 2 shows a very fast decay to a small offset level and displays no discernible oscillations. A single-exponential fit to the data starting at the peak of the signal yields a decay time of 63 fs and a ∼10% offset level. A fit starting after 60 fs, well after the instrument response, yields an almost identical decay time of 59 fs. This indicates that there is no coherence spike on the signal, which can occur when the pulse duration is shorter than the electronic dephasing time.[40,41] Due to the *E*-field squared nature of the signal, the decay is proportional to $\sim\exp(-2t/T_{pop})$, and the 60 fs decay time therefore corresponds to a population decay time of $T_{pop} = 120$ fs. This is in good agreement with reported energy-transfer times.[15−18] A double-exponential decay improves the fit only slightly and yields population decay times of 88 fs (63%) and 153 fs (37%). The signal shows a small increase on the picosecond time scale (see inset).

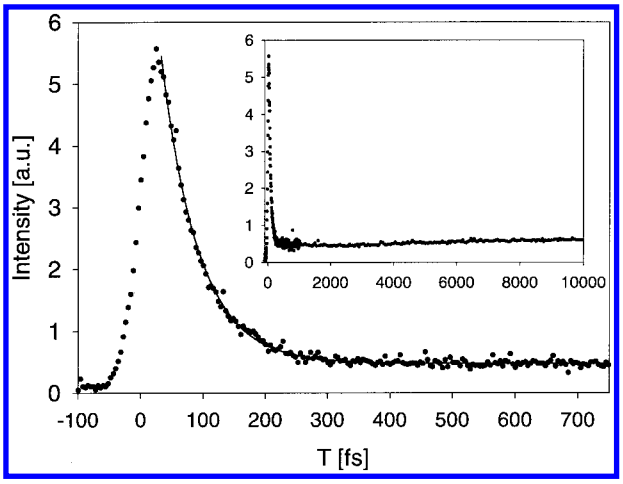

Figure 2. Transient grating signal measured at 800 nm (total band). The inset shows the signal up to 10 ps. The solid line is a fit with $t =$ 60 fs or $T_{pop} =$120 fs.

The offset may have two causes: (1) After energy transfer to P* has taken place there is some P* excited-state absorption in the 800 nm region; absorption difference spectra show a net absorption increase with a peak around 810 nm during the lifetime of P*. This feature is particularly clear in, for example, the species-associated spectrum of ref 12, whereby it should be noted that a bleaching due to the P_+ state might even lead to an underestimate of the magnitude of the excited-state absorption. The grating associated with this absorption is expected to be shifted by π with respect to the original grating, since what was initially an absorption decrease is now an absorption increase. Furthermore, (2) the direct formation of $P^+B_A^-$ or $B_A^+H_A^-$, which competes with energy transfer,[22−25] leaves the original B ground-state grating intact. Because of the π phase shift of the P* grating, the two gratings are expected to interfere destructively. On the longer time scale, when electron transfer from P to H has occurred, the transient grating signal will be due to the electrochromatic shift of the 800 nm band upon P^+ formation.

To obtain spectral resolution within the 800 nm band, the decay of the transient grating was also measured with interference filters placed behind the sample; see Figure 1 for the detection window of the filters. At 790 nm (Figure 3, white squares) the decay is slightly slower than that of the total band: $T_{pop} =$ 130 fs. At 810 nm (Figure 3, black circles), it is significantly faster: $T_{pop} =$ 80 fs. To make sure that this difference in the decay times is not due to the P* excited-state absorption which peaks around 810 nm, we tried to fit the signal with a function that would describe such a process, and we concluded that P* excited-state absorption is too small to affect the lifetime of decay. The offset level at 810 nm is slightly larger than that at 790 nm and of the total band, and both signals increase on the picosecond time scale (see inset). The time constant of this increase is about 15 ps, or $T \sim$ 30 ps.

Three-Pulse Photon Echo Peak Shift of the 800 nm Band. The echo peak shift as a function of population time T is plotted in Figure 4 on a logarithmic time scale; the inset shows the decay up to 400 fs on a linear scale. The initial peak shift is 20 fs, which is similar to the initial peak shifts of 24 fs observed in LH1 and LH2.[36] This shows that the coupling strengths of these systems are similar. Note however that a shorter excitation pulse as used in this study (27 fs vs 35 fs) leads to a slightly lower initial peak shift; see refs 34 and 35 in line with the observed peak shift. The decay of the peak shift curve displays three different time scales: the initial decay to a plateau of ∼10 fs peak shift occurs in ∼50 fs, this is followed by a slower decay to a peak shift of 2−2.5 fs, and a remarkable *increase* of the peak shift takes place on a picosecond time scale.

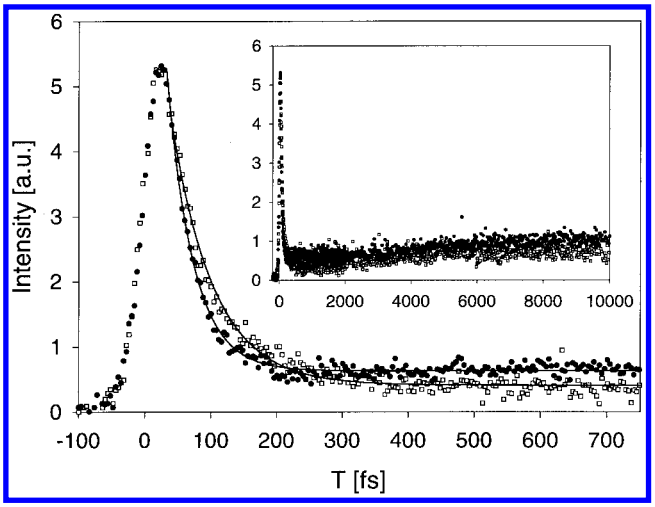

Figure 3. Transient grating signal at 810 nm (black circles) and 790 nm (white squares). The solid lines are fits with $t =$ 40 and 65 fs or $T_{pop} =$ 80 and 130 fs, respectively. The inset shows the signal up to 10 ps.

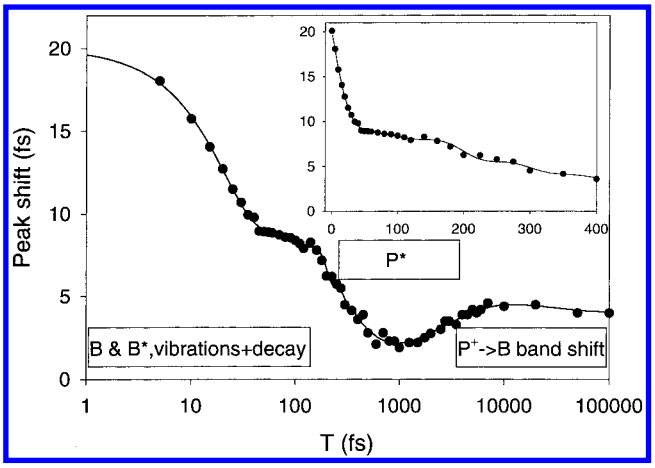

Figure 4. Echo peak shift of the total band on a logarithmic time scale. The inset shows the initial part of the decay on a linear scale. The solid line is a fit to eq 1 with $a_1 =$ 1.2 fs, $t_d =$ 94 fs, $t_6 =$ 240 fs, $a_6 =$ 12.6 fs, $t_7 =$ 2.8 ps, $a_7 =$ 4 fs, $t_8 =$ 30 ps, and $a_8 =$ 0.8 fs; see text.

The peak shift decay has been shown to be linear with the time correlation function of the electronic transition frequency, $M(t)$, for times longer than the bath correlation time.[33] For shorter times the peak shift and $M(t)$ are related in a more complicated way. $M(t)$ in general is written as a sum of Gaussian, exponentials, and damped cosine terms. To get, however, an idea of the time constants involved, it is instructive to perform a direct (linear) fit of the peak shift curve to a sum of exponentials and damped oscillations.

Vibrations in the ground and excited state modulate the electronic transition frequency and will show up in the peak shift curve as (damped) oscillations. Though the decay of the transient grating signal is too fast to observe any oscillations, resonance Raman experiments[42] on the 800 nm band have shown the presence of ground-state vibrations at 117,177, 212, 332, 355, and 384 cm^{-1} with relative intensities of 1:4.1:3.7: 1.8:1.4:1.5. Other frequencies have lower Raman intensity and/or fall outside the excitation window of our pulse (∼630 cm^{-1}). In the fit we have included the vibrations as five damped cosines with fixed frequencies, merging the 332 and 355 cm^{-1} frequen-

cies into one cosine with an average frequency of 340 cm^{-1}. The fit furthermore includes two exponential decays and a rise term:

$$f(t) = [\sum_{i=1}^{5} a_i \cos(\omega_i + \phi_i)] \exp(-t/\tau_d) + a_6 \exp(-t/t_6) + a_7(1 - \exp(-t/t_7)) + a_8 \exp(-t/t_8)$$

A good fit (solid line in Figure 4) is obtained with the relative amplitudes of the vibrations fixed to those of the Raman data with a_1 =1.2 fs (i.e., $a_2 = 4.9$, $a_3 = 4.4$, $a_4 = 3.8$, and $a_5 = 1.8$) and a damping time of $\tau_d = 94$ fs. The vibrations are needed to describe the plateau around 100 fs and account for the major part of the initial decay to the plateau level. The time constant of the first exponential is $t_6 = 240$ fs, with an amplitude of $a_6 = 12.6$ fs. When an extra exponential component is included with a decay time identical to the damping time of the cosines, its amplitude is 4 fs. This changes a_1 to 2.2 fs, t_6 to 276 fs, and a_6 to 10.7 fs. The rise term has a time constant of $t_7 = 2.8$ ps and an amplitude of $a_7 = 4$ fs. The small decay after ~10 ps is fitted with a time constant of $t_8 = 30$ ps and an amplitude of $a_8 = 0.8$ fs.

To summarize, although there is some freedom in the fit, especially in the first part due to the nine free parameters there, it is clear that the plateau around 100 fs and the initial decay of the peak shift are due to vibrations that are damped on a ~100 fs time scale. We find that the decay of the peak shift to ~2 fs at ~1 ps cannot be described by oscillations and is best fitted by an exponential decay of ~240 fs, which accounts for at least 50% of the total decay. A minor ~100 fs exponential decay can be fitted but is found to be canceled by an increased amplitude of the oscillations.

Before we start the actual construction of $M(t)$ based on these findings and simulate the peak shift, we need a better qualitative understanding of the data in order to be able to construct a physically correct $M(t)$.

Energy Transfer. How is energy transfer expected to show up in the peak shift decay curve of the B pigments? Energy transfer may not have any effect on the population which evolves in the ground state between the second and third pulse, but the excited-state population decays as the energy is transfered. Previous experiments have shown that if the product state is resonant with the laser, for instance B850−B850 energy transfer or B800−B850 transfer in the LH2 complex (here the B850* excited-state absorption is around 800 nm), then the energy transfer shows up in peak shift measurements.[36,37] Before we discuss the initial portion of the peak shift, we turn briefly to the last part. An increase in peak shift, i.e., an increase in rephasing capability, has to our knowledge not been observed in any other system. The 2.8 ps time constant indicates that it is correlated with charge separation. Why should it lead to an increase in the peak shift? Also, we see that the asymptotic peak shift, which reflects both the ratio of the homogeneous and inhomogeneous width and the total width[33,44,45] is not zero. From this and from the fact that the oscillations are damped with the time of energy transfer, it follows that between 100 fs and 1 ps, where the peak shift is lower than the asymptotic value, the photo echo probes something else than the dynamics on B, i.e., a state that is characterized by a peak shift of zero.

As briefly discussed in the transient grating section, P has an excited-state absorption around 810 nm, and it will be this state that is probed after energy transfer from B to P has taken place. If there is no frequency grating present on P*, the third pulse cannot induce rephasing, and only a free induction decay signal, i.e., with zero peak shift, is induced. The large decay of the peak shift between 100 fs and 1 ps to almost zero peak shift can therefore be explained by the disappearance of echoes from B due to the decay of the B gratings and the appearance of a free induction decay signal from P* due to P excited-state absorption. The subsequent increase of the peak shift with the 2.8 ps time constant occurs because with charge separation the 800 nm band shifts, and peak-shifted echoes from B reappear. This explanation is schematically presented by the boxes in Figure 4.

Though the damping time of the vibrations does correlate with the time of energy transfer, the exponential decay time of ~250 fs does not correlate with reported energy-transfer times, including those of our own transient grating data. This unexpectedly slow exponential decay of the rephasing capability may be due to (1) the interference of echoes from persisting B ground-state contribution, due to direct $P^+B_A^-$ or $B_A{}^+H_A^-$ formation,[22−24] with nonrephasing signals from P*. If direct charge separation from B_A occurs after the first two pulse interactions, forming either $P^+B_A^-$ or $B_A{}^+H_A^-$, the B_A ground-state contribution is left intact. The third pulse will then interact with the ground-state grating, and after rephasing a peak-shifted echo will be produced that tracks the dynamics on the ground state of B_A. There may, however, also be other explanations: (2) If there is strong electronic coupling between B and P, there may be a frequency correlation between B and P, creating a frequency grating on P* after energy transfer and therefore rephasing capability. Or (3) an unexpectedly large direct excitation of the upper exciton band of P, P_+, may, after internal conversion to P_-, create a frequency grating on P* and therefore rephasing capability.

To address this issue, we have done post-sample frequency resolved peak shift measurement on the 800 nm band. If the first explanation, i.e., the formation of a direct charge-separated state, is correct, then we expect to see on the red side, where P* is preferentially probed, a faster decay than in Figure 4, because with the interference filter any contributions from B_A are eliminated and P* would only give free induction decay signal. On the blue side we expect to see dynamics of the B ground state: direct electron transfer has been reported to occur mainly upon excitation on the blue side of the band, i.e., probably involves only the B_A pigment in the active branch.[25] Moreover, because there is only a minor amount of P* excited-state absorption around 790 nm, the P* absorption induced upon blue excitation is shifted outside the detection window. Experiments at 790 nm are therefore a way to study B ground-state dynamics, without the interference of P*.

If either of the latter two explanations, i.e., coupling between B and P pigments or transfer of frequency grating to P* after the excitation of P_+, is correct, then on the red side, where the P excited-state absorption peaks, we would see a decay of the peak shift slower than the energy-transfer time, as in Figure 4, because of the correlation between the initial gratings and that created on P. On the blue side, where there is hardly any P* absorption, we would expect the echo amplitude signal to disappear as the B excited state decays. (Note that this is already in disagreement with the observation of the small transient grating signal on a time scale longer than energy transfer.)

Echo Peak Shift at 790 and 810 nm. The frequency-resolved peak shifts are shown in Figures 5 and 6. The peak shift around 810 nm (see Figure 5) shows a behavior that is similar to that of the total band, except that the vibrational beat around 100 fs is more pronounced and the subsequent decay to zero peak shift is faster, ~130 fs. The peak shift around 790

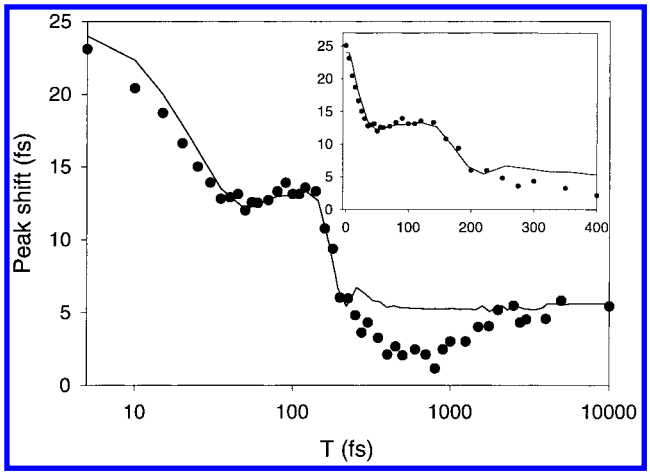

Figure 5. Echo peak shift at 810 nm on a logarithmic time scale. The inset shows the initial part of the decay on a linear scale. The solid line is a simulation; see Table 2 for parameters of $M(t)$. The data points between ~100 fs and ~4 ps have been ignored in the simulation since they arise from P* and therefore do not contain information on B; see text.

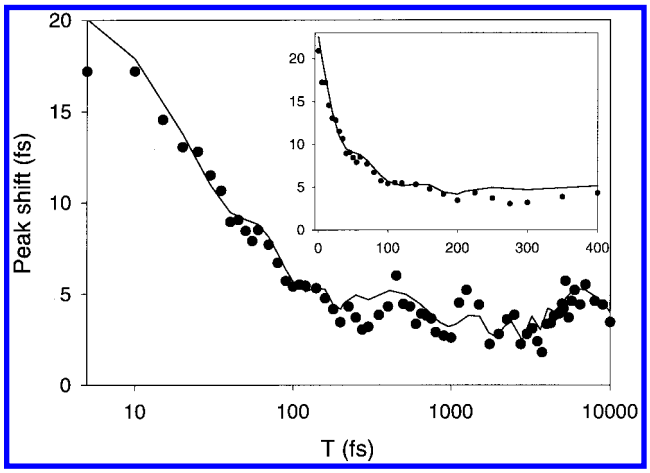

Figure 6. Echo peak shift at 790 nm on a logarithmic time scale. The inset shows the initial part of the decay on a linear scale. The solid line is a simulation; see Table 1 for parameters of $M(t)$.

nm (Figure 6) is different: it does not display the prominent beat around 100 fs, but rather decays to a level of about 4 fs in 50−60 fs. During this decay, but certainly also after 100 fs and even up to 10 ps, the peak shift oscillates and there is no rise in peak shift after 1 ps.

These results are in line with the first explanation, i.e., direct charge separation from B state, but in disagreement with the second two. In the region where predominantly excited-state absorption of P is observed (810 nm), the peak shift decays to a minimum of 1−2 fs with a time constant close to that of energy transfer and no rephasing capability of P* is observed, whereas where this absorption is absent (790 nm), a peak shift is observed that displays dynamics up to 10 ps.

Simulation of the 790 and 810 nm Peak Shifts. The peak shift curves are simulated (solid lines in Figures 5 and 6) by constructing a correlation function $M(t)$, which should also be able to reproduce the absorption spectrum. To get a first idea of $M(t)$, the data were fitted to a sum of exponentials and damped cosines as for the total band peak shift of Figure 4. The amplitudes were subsequently recalculated to coupling strengths and the phases of the oscillations shifted by 20 fs in order to match the data. In addition, to independently check whether the frequencies of the oscillations in the data agreed with those of the Raman data, we applied a linear prediction

TABLE 1: Parameters of $M(t)$ for the Simulation of the 790 nm Peak Shift Data Shown in Figure 6[a]

790 nm	$\langle\Delta\omega^2\rangle^{1/2}$ (cm^{-1})	t (fs)	ν (cm^{-1})	t_d (fs)	ϕ (rad)
oscillation 1	40		3−4	20000	1.4
oscillation 2	20		36	3000	2.9
oscillation 3	70		177[b]	80	0.2
oscillation 4	50		212[b]	130	1.9
oscillation 5	60		340[b]	130	−2.9
oscillation 6	140		384[b]	80	−0.1
oscillation 7	130		569[b]	80	−0.5
oscillation 8	100		630[b]	80	1.4
Gaussian	85	60			
Γ_{inhom}	55				

[a] Coupling strengths $\langle\Delta\omega^2\rangle^{1/2}$ in cm^{-1} of the oscillations, Gaussian, and inhomogeneous components; time constant of the Gaussian component ($\Delta^2 \exp(-t^2/\tau^2)$) in fs; frequency ν of the oscillations in cm^{-1}; damping time t_d of the oscillations in fs; phase ϕ of the oscillations in rad. [b] A fixed parameter.

routine to the 790 nm data from 0 to 2 ps. This yielded frequencies of 367 cm^{-1} with a damping time of 40 fs, of 313, 242, 143, and 88 cm^{-1} with damping times between 175 and 680 fs, and of 32 cm^{-1} with a damping time of 3 ps. We considered these frequencies close enough to those of the Raman data,[42] to justify using the Raman frequencies in fitting and simulating the data. Since 790 nm is on the high-energy side of the absorption band, we included higher frequency (569 and 680 cm^{-1}) modes from the Raman data. Also, to describe the oscillations between 300 fs and 1.3 ps, we added a 36 cm^{-1} mode as well as a 3.6 cm^{-1} mode. The latter we added in order to describe a small, slow exponential decay found when the data were fitted up to 2 ps and the peak at around 6 ps.

Table 1 shows the parameters used to obtain the simulation of the 790 nm data of Figure 6 (solid line). The initial and the asymptotic peak shift depend on the ratio of the homogeneous and inhomogeneous line widths and the total line width. The decay of the peak shift, due to homogeneous dephasing processes, was simulated with a Gaussian decay with a time constant of 60 fs and a coupling strength of 85 cm^{-1}. The inhomogeneous width is 55 cm^{-1}, which is in exact agreement with the number reported by Cherepy et al.[42] This corresponds, after multiplication with $\sqrt{8 \ln 2}$, to a fwhm of 130 cm^{-1}. The 80 fs damping time of the vibrations is reasonably well determined by the data and the damping time of the 212 and 340 cm^{-1} modes, now set at 130 fs, less so. The feature at 450 fs could have been fitted by increasing the damping times to a few hundred femtoseconds. This does, however, lead to a poorer fit at earlier times. Though this might imply that several of the modes require both a short and a long damping time, we have rather restricted ourselves here to describing the main features of the data. With these parameters an absorption spectrum is calculated (see Figure 7) that is slightly narrower than the experimental spectrum.

To simulate the 810 nm peak shift data which has contributions from the P* excited-state absorption (the decay of peak shift to zero in 140 fs as discussed earlier is due to interference of free induction decay/echoes from P* absorption) and to obtain the correct parameters for $M(t)$ of B, we have attempted to eliminate the P* echoes from the simulation in the following way. Assuming that the inhomogeneous width at 810 nm is the same as at 790 nm, 55 cm^{-1}, and keeping the relative amplitude and the phase of the vibrations the same, the coupling strength and rate constant of the exponential process and the total coupling strength of the vibrations are varied. Only the part of the curve between 0 and 130 fs (the maximum of the

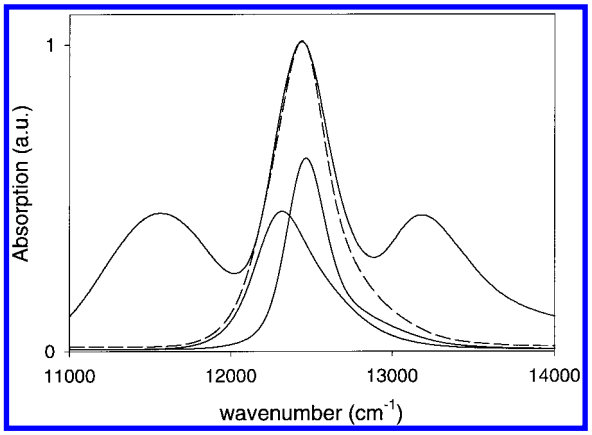

Figure 7. Experimental absorption (solid line) and the absorption spectra calculated from the $M(t)$ functions at 790 and 810 nm, shifted to 802 and 811.5 nm, respectively. For both spectra the lifetime broadening is included (i.e., the excited-state lifetime of 130 and 80 fs, respectively); see Tables 1 and 2 for all other parameters. The dashed line is the sum of the two simulated spectra.

TABLE 2: Parameters of $M(t)$ for the Simulation of the 810 nm Peak Shift Data Shown in Figure 5[a]

810 nm	$\langle\Delta\omega^2\rangle^{1/2}$ (cm^{-1})	t (fs)	ν (cm^{-1})	t_d (fs)	ϕ (rad)
oscillation 1	20		117[b]	80	−3.7
oscillation 2	80		177[b]	80	0.9
oscillation 3	110		212[b]	80	0.1
oscillation 4	160		340[b]	80	1.3
oscillation 5	130		384[b]	80	4.1
exponential	125	90			
Γ_{inhom}	55[b]				

[a] Coupling strengths $\langle\Delta\omega^2\rangle^{1/2}$ in cm^{-1} of the oscillations, exponential, and inhomogeneous components; time constant of the exponential component in fs; frequency ν of the oscillations in cm^{-1}; damping time t_d of the oscillations in fs; phase ϕ of the oscillations in rad. [b] A fixed parameter.

vibrational beat) and the asymptotic peak shift at $T > 4$ ps were simulated. Increasing the coupling strength or the rate constant of the exponential leads to a decrease of the residual peak shift, but on the initial peak shift they each have opposite effects. Therefore, they are reasonably well determined once we choose the inhomogeneous width to be 55 cm^{-1}. We obtained 125 cm^{-1} and ~90 fs for the coupling strength and time constant, respectively. It was not possible to obtain a simulation of the data if the exponential decay was replaced by a Gaussian decay with a correlation time of about 90 fs, nor with a faster or slower correlation time. This is probably because the tail of the decay of a Gaussian is faster than that of an exponential, and we could therefore not simulate the relatively gradual decrease from the plateau level to the asymptotic level. The simulated peak shift curve is shown as the solid line in Figure 5; see Table 2 for the parameters. The absorption spectrum that we calculate from these parameters (see Figure 7) is broader and more asymmetric than that from the 790 nm parameters but only slightly broader than the experimental spectrum.

With the 810 nm simulated spectrum shifted to 811.5 nm and the 790 nm spectrum to 802 nm, the experimental spectrum is very well reproduced by the sum of the two. These positions agree very well with the positions of the B_A and B_B absorption bands at 800−802 and 812 nm, respectively, as determined from low-temperature absorption difference spectra.[45] It is however obvious that both pigments contribute to the peak shift measured at 790 nm, since that is at the high-energy side of both, and the simulated spectrum therefore cannot be ascribed to B_A only. Nevertheless, the correlation function $M(t)$ is capable of describing both the peak shift curves and the absorption spectra in a satisfactory manner, and we are therefore confident that it captures the dynamics of the B pigments.

Discussion

The echo peak shift curve of the 800 nm band displays the dynamics of the B pigments but is to a large extent also determined by the effects of P* and radical pair formation in the RC on the 800 nm band.

Energy Transfer in the Echo Peak Shift Curve. From the frequency-resolved peak shift measurement, we conclude that in the case of the peak shift at 810 nm it is the appearance of nonrephasing, free induction decay signals of P* that causes the peak shift to decay on the time scale of energy transfer. The time constant of this decay (240 fs) of the entire 800 nm band is slower than the actual energy-transfer time due to the mixture of echoes from both P* absorption and the B ground-state that can only be disentangled in the frequency-resolved experiments.

That P* absorption gives rise to an almost zero peak shift at 1 ps demonstrates that there is no transition frequency correlation between the 800 nm band and P_- and that around 810 nm the upper exciton band of P, P_+, is not excited to a significant extent. Rather than to the P excited-state absorption, the net absorption increase on the red side of the 800 nm band upon P* formation has recently been interpreted as a blue shift of B_B, based on a comparison between native and chemically treated RC's.[19] The observation of an almost zero peak shift is in disagreement with this interpretation, since it can only be due to a grating that is not in any way related to the original B ground- or excited-state gratings. The chemical treatment with sodium borohydride must therefore have affected not only B_B, as assumed by the authors,[19] but also P.

The increase of the peak shift with a time constant of 2.8 ps can be explained by a decay of P* as the charge-separated state is formed and the subsequent recovery of the echo signal from the B ground-state, which as we discussed earlier has a nonzero asymptotic peak shift. The increase may also be due to the electrochromic shift of B band due to formation of P^+H^-, which unlike P^+B^- is within the spectral window of our laser pulse and may give echoes.

At 790 nm the P* excited-state absorption is negligible, and indeed no exponential decay of the peak shift curve is observed that might be related to energy transfer. Note that only a B population is expected to give rise to a frequency grating and rephasing capability. Therefore, to explain this we ascribe the rephasing capability after ~100 fs to a persistent B ground-state grating due to the direct formation of a B cation or anion, i.e., of the state $P^+B_A^-$ or $B_A^+H_A^-$ without involvement of P*.[22−24] This occurs in about 20% of all RC's and probably in about 40% upon blue excitation.[22−24] These states have been observed to have a lifetime of ~14 ps at room temperature in wild-type RC's[22] and 6.5 ps at 77 K in M210 mutants.[23] We do not observe a decay related to this because the subsequently formed $P^+H_A^-$ state again leads to a B ground-state grating, and the information in the echo peak shift remains the same. The reason we do not see the rise in the peak shift after 1 ps at 790 nm is because there is much less contribution from P* free induction decay and the B ground state is preferentially probed after the energy/electron transfer takes place.

At 810 nm, after eliminating the contribution of P* from the analysis, we obtain a 90 fs exponential decay of rephasing capability. We ascribe this component to a dephasing process of similar nature as the 60 fs Gaussian decay in the 790 nm

peak shift, i.e., to dephasing due to small librational motions of the protein with amplitude Δ. A Brownian ocillator would provide a better description of the full time range than a simple exponential. However, as we have shown[33,34] that the initial portion of the peak shift is rather insensitive to whether the underlying correlation function is exponential or Gaussian, given this, the additional complexity of a Brownian oscillator fit does not seem warranted.

Homogeneous Line Width. The coupling strength Δ of the Gaussian decay in $M(t)$ at 790 nm is 85 cm^{-1}. The 60 fs time constant of the Gaussian corresponds to an inverse correlation time ($t_c = \int dt\, M(t)$) of $1/t_c = 1/54$ fs $= \Lambda = 98$ cm^{-1}. We can now calculate the fwhm of the homogeneous line width, using as definition for the homogeneous line width that line width caused by fast dynamics of the solvent or protein environment. Since we are neither in the fast ($\Lambda/\Delta \gg 1$) nor in the slow ($\Lambda/\Delta \ll 1$) bath modulation limit, we calculate the fwhm of the homogeneous line width according to ref 46 and obtain $\Gamma_{hom} = 118$ cm^{-1}, which is considerably line narrowed. Though the analysis of the 810 nm curve is hampered by the P* echo that appears after energy transfer has taken place, it is clear from the large vibrational beat around 100 fs that the initial part of the peak shift decay is dominated by vibrations rather than by a fast ~50−60 fs decay. Furthermore, the 90 fs process seems to be an exponential process rather than a Gaussian. When we calculate the corresponding fwhm of the homogeneous line width, we have $1/t_c = \Lambda = 60$ cm^{-1} and $\Delta = 125$ cm^{-1}, i.e., near the slow modulation limit, and obtain[46] fwhm of $\Gamma_{hom} = 250$ cm^{-1}.

The differences in the correlation functions of the 790 and 810 nm peak shifts are therefore both the time scale of the nuclear dynamics, i.e., the bath correlation time, and the coupling strength which are both ~1.5 times faster and weaker at 790 nm than at 810 nm. It is not likely that these differences are an artifact of the frequency-resolved technique. First of all, the reorganization energy associated with the Gaussian component is very small (20 cm^{-1}), much smaller than the spectral width of the 790 nm filter, and the fast initial decay is therefore not due to a relaxation in/outside the detection window. Furthermore, similar frequency-resolved echo experiments on the 800 nm band in LH2 antenna complexes[61] did not reveal such a dependence on the detection wavelength. We conclude that there are subtle differences in the dynamics on the blue and red side of the 800 nm band, which might be attributed to differences in the protein environment of the B_A and B_B pigments, respectively.

From modeling Raman cross sections upon excitation at 800 nm, Cherepy et al.[42] concluded that pure dephasing is best described by a Gaussian with a standard deviation of 85 cm^{-1}, assuming the slow modulation limit. Although this appears to correlate with the coupling strength of our Gaussian component at 790 nm, the fact that the correlation time of the Gaussian is only 54 fs, or 98 cm^{-1}, shows that the nuclear/bath dynamics are actually not in the slow modulation limit. The resulting line shape from the 790 nm correlation function is therefore more Lorentzian and the fwhm is narrower than that of Cherepy et al.,[42] i.e., 118 vs 196 cm^{-1}. The line shape at 810 nm, which is closer to the slow modulation limit and therefore more Gaussian, is slightly broader than that of ref 42. These differences may arise from the fact that in that study only 800 nm excitation was used, and therefore a convolution of the two line shapes was observed. As mentioned earlier, the standard deviation of inhomogeneous width of each of the transitions is equal to those of ref 42 at room temperature, i.e., 55 cm^{-1}. The positions of the two simulated absorption spectra, at 811.5 and 802 nm, are more similar to those of their 95 K simulation than that at room temperature.[42] It is interesting to note that the absorption spectra in our simulation, with their relative shift and the red spectrum being broader than the blue one, are reminiscent of the low-temperature absorption spectrum, which has a shoulder on the low-energy side. We expect therefore that the low-temperature absorption spectrum can be simulated without major adjustments to $M(t)$, i.e., by incorporating the temperature effect on the homogeneous line width only, without changing the inhomogeneous width or the position within the band. The shoulder in the low-temperature absorption spectrum is absent, or much less pronounced, in carotenoidless strains.[47] This might suggest that the carotenoid, which is located near B_B, has an influence on the dynamic properties that cause the broad homogeneous line width, i.e., the longer correlation time and the larger coupling strength.

Energy Transfer. The use of interference filters to disperse the signal behind the sample results in a reasonably high-frequency resolution without loss of time resolution around time zero. This is due to the homodyned nature of the transient grating experiment, as opposed to the heterodyned nature of pump−probe experiments, which can cause problems (oscillations, signals at negative delay times) when the pulse length is of the same order as the electronic dephasing time. The combination of high time and frequency resolution within the 800 nm band allowed the observation of a shorter lifetime of the excited state at 810 nm (80 fs) than at 790 nm (130 fs). Wavelength-dependent kinetics have been observed earlier, though on the more extreme sides of the 800 nm band, but were ascribed to direct excitation of the P^+ state[18,24] or coherent excitation of the B* and P^+ states[24] or were observed at low temperature in the heterodimer mutant.[21] From the analysis of the peak shift data it is clear that at both 790 and 810 nm the decay is due to B*. We conclude therefore that energy transfer to P is faster upon red than upon blue excitation.

The bath correlation time is about 90 fs on the red side of the 800 nm band; therefore, nuclear rearrangement is not completed on the time scale of energy transfer. At the very least, time-dependent spectral overlaps[48] will be needed to calculate the energy-transfer rate. More likely, a more sophisticated approach including the effects of coherence transfer[49] and using a model for the electronic coupling that allows for orbital overlap[50] will be required. The role of orbital overlap in B to P energy transfer has been suggested by Boxer and coworkers[18,21] as a result of their comparison of the wild-type and heterodimer mutant. Further, the direct charge separation pathway from B* indicates that coupling other than pure Coulombic is of importance in the RC. A very crude estimate of the overall (Franck−Condon weighted) coupling strength V can be obtained from the Forster strong coupling expression $n = 4V/c$ using the observed 1/(80 fs) rate. Since n actually describes an oscillating process and corresponds to the time needed to transfer all population from one state to the other, i.e., half a period of oscilation, we need to calculate the corresponding value of our exponential rate, which is $n = 1/(136$ fs). Note that we have to assume that the oscillatory population is rapidly damped on the acceptor level, for instance in the case of the upper exciton level of P, P_+ as acceptor, due to a fast relaxation of P_+ to P_-. With $n = \sim 1/(136$ fs) this gives $V = 61$ cm^{-1}. The observation of a 90 fs bath correlation time suggests dephasing is concurrent with the formation of P_- and is therefore consistent with the free induction decay signals from P*. Finally, it will be of interest to determine whether the

vibrational motions play a mechanistic role in the energy transfer or simply act as spectators in the transfer.

Slow Oscillations. In the peak shift curve measured at 790 nm slow oscillations with a period of about 1 and 10 ps are observed. Although the simulation between 0.3 and 1.5 ps is not perfect (it could have been improved by a longer damping time of the higher frequency modes as mentioned above or by adding an extra low-frequency mode to $M(t)$), its essential features are reproduced by the underdamped 36 cm^{-1} mode. In hole-burning experiments on pigment−protein complexes usually a phonon sideband is observed which is ascribed to a broad distribution of low-frequency motions of the protein with a mean frequency of 30 cm^{-1}; see e.g. refs 52 and 53. Unfortunately, no hole-burning spectra have been reported for the accessory Bchl pigments. Small low-frequency motions of the protein/solvent also cause the initial fast decay of the peak shift. However, such low-frequency modes are usually not observed as an oscillation of the peak shift at longer times, since they have a broad distribution of frequencies that will dephase quickly. In order for a mode to show up as a modulation of the peak shift, it must be a coherent, well-defined motion. Coherent low-frequency modes of 15 $^{-}$ and ∼80 cm^{-1} have also been observed in the stimulated emission of P,[54,55] and resonance Raman data of P revealed a 36 cm^{-1} mode.[56] Molecular dynamics calculations have also yielded several slow motions that are correlated on a picosecond time scale. For example, Alden et al.[57] studied the effect of the orientation of the OH dipole of tyrosine M210, which is located near both P and B_A, on the electronic states of P and B_A. They found that the oscillation frequency of the orientation of the OH dipole had a major peak at 130 cm^{-1} in the PB_A ground state, which shifted to 260 cm^{-1} in the $P^+B_A^-$ state, and a distinct peak around 3 cm^{-1}. Gehlen et al. observed underdamped oscillations with a period of a few picoseconds in the distance between pigments in the RC in molecular dynamics simulations, which were speculated to have a possible role in the electron-transfer process.[58]

The 30 ps Process. On a long time scale, a 30 ps decay of the peak shift of the total band is observed (see Figure 4; the frequency-resolved peak shift curves were measured only up to 10 ps, see Figures 5 and 6). Though it is only a small decay of the asymptotic peak shift, from 4.8 to 4 fs, it is accompanied in the transient grating signals by a relatively large rise, most pronounced in the frequency-resolved TG measurements; see Figure 3. Kinetics on this time scale in absorbance difference or fluorescence measurements are usually ascribed to relaxations of the radical pair state, for which a wide range of time scales has been reported, from ∼20 ps to tens of nanoseconds; see e.g. refs 12, 59, and 60. That the rise is larger in the frequency-resolved TG signals indicates that an increase of the electrochromatic band shift occurs. The fact that the rephasing capability decreases suggests that, if we interpret it as a decrease of the inhomogeneous width and therefore a decrease in the distribution of sites, a change in the environment of B has occurred. A change in the environment of B may for example be an adaptation of the protein in response to the formation of $P^+H_A^-$, which increases the effect of the electric field of P^+ on B and stabilizes the radical pair state.

Conclusion

We have determined the ultrafast dynamics of the accessory pigments in the bacterial RC. By measuring frequency-resolved echo peak shifts, we were able to demonstrate differences in the protein dynamics on the blue and red side of the 800 nm absorption band, which may be related to differences in the protein environment of the B_A and B_B pigments. On the red side the energy transfer is faster and occurs from a coherent state, since the bath correlation time is at least as long as the energy-transfer time. The bath dynamics and the energy-transfer time decrease and increase, respectively, at shorter wavelengths, and therefore the nature of the energy-transfer process and possibly also the coupling to product states change over the band. The peak shift data at 790 nm may provide support for direct charge separation from B, without involvement of P*.[22−24] The versatility of the peak shift technique for characterizing slow dynamics of pigment−protein complexes is illustrated by the observation of very low-frequency coherent oscillations and a long-time decrease of the peak shift in ∼30 ps. To interpret these results quantitatively at a higher level, a detailed theory incorporating the effects of energy and electron transfer on the nonlinear response functions is required.

Acknowledgment. We thank Julia Popov for the preparation of the reaction center samples and dr. F. van Mourik for the suggestion of the frequency-resolved experiments. R.A. and G.R.F. also thank Mino Yang for many helpful discussions. This work was supported by a grant from the National Science Foundation.

References and Notes

(1) Parson, W. W. In *Chlorophylls*; Scheer, H., Ed.; CRC Press: Boca Raton, FL, 1991; p 1153.

(2) Woodbury, N. W.; Allen, J. P. In *Anoxygenic Photosynthetic Bacteria*; Blankenship, R. E., Bauer, C. E., Eds.; Kluwer Academic Publishers: Dordrecht, The Netherlands, 1995; p 527.

(3) Fleming, G. R.; van Grondelle, R. *Phys. Today* **1994**, *47*, 48.

(4) Allen, J. P.; Feher, G.; Yeates, T. O.; Komiya, H.; Rees, D. C. *Proc. Natl. Acad. Sci. U.S.A.* **1987**, *84*, 6162−6166.

(5) Chirino, A. J.; Lous, E. J.; Huber, M.; Allen, J. P.; Schenck, C. C.; Padock, M. L.; Feher, G.; Rees, D. C. *Biochemistry* **1994**, *33*, 4584−4593.

(6) Holzapfel, W.; Finkele, U.; Kaiser, W.; Oesterhelt, D.; Scheer, H.; Stilz, H. U.; Zinth, W. *Proc. Natl. Acad. Sci. U.S.A.* **1990**, *87*, 5168−5172.

(7) Schmidt, P. M.; Arlt, T.; Hamm, P.; Huber, H.; Nagele, T.; Wachtveitel, J.; Meyer, M.; Scheer, H.; Zinth, W. *Phys. Rev. Lett.* **1994**, 116.

(8) Kirmaier, C.; Laporte, L.; Schenck, C. C.; Holten, D. *J. Phys. Chem.* **1995**, *99*, 8910.

(9) Heller, B. A.; Holten, D.; Kirmaier, C. *Science* **1995**, *269*, 940−945.

(10) Arlt, T.; Bibikova, M.; Penzkofer, H.; Oesterhelt, D.; Zinth, W. *J. Phys. Chem.* **1996**, *100*, 12060.

(11) Holzwarth, A. R.; Muller, M. G. *Biochemistry* **1996**, *35*, 11820−11831.

(12) Van Stokkum, I. H. M.; Beekman, L. M. P.; Jones, M. R.; Van Grondelle, R. *Biochemistry* **1997**, *36*, 11360−11368.

(13) Breton, J.; Martin, J.-L.; Migus, A.; Antonetti, A.; Orszag, A. *Proc. Natl. Acad. Sci. U.S.A.* **1986**, *83*, 5121−5125.

(14) Breton, J.; Martin, J.-L.; Fleming, G. R.; Lambry, J.-C. *Biochemistry* **1988**, *27*, 8276−8284.

(15) Wynne, K.; Haran, G.; Reid, G. D.; Moser, C. C.; Dutton, P. L.; Hochstrasser, R. M. *J. Phys. Chem.* **1996**, *100*, 5140−5148.

(16) Haran, G.; Wynne, K.; Moser, C. C.; Dutton, P. L.; Hochstrasser, R. M. *J. Phys. Chem.* **1996**, *100*, 5562−5569.

(17) Jonas, D. M.; Lang, M. J.; Nagasawa, Y.; Joo, T.; Fleming, G. R. *J. Phys. Chem.* **1996**, *100*, 12660−12673.

(18) Stanley, R. J.; King, B.; Boxer, S. G. *J. Phys. Chem. B* **1996**, *100*, 12052−12059.

(19) Vulto, S. I. E.; Streltsov, A. M.; Shkuropatov, A. Y.; Shuvalov, V. A.; Aartsma, T. J. *J. Phys. Chem. B* **1997**, *101*, 7249−7255.

(20) Jean, J. M.; Chan, C.-K.; Fleming, G. R. *Isr. J. Chem.* **1988**, *28*, 169−175.

(21) King, B. A.; Stanley, R. J.; Boxer, S. G. *J. Phys. Chem. B* **1997**, *101*, 3644−3648.

(22) Lin, S.; Taguchi, A. K. W.; Woodbury, N. W. *J. Phys. Chem. B* **1996**, *100*, 17067−17078.

(23) Van Brederode, M. E.; Jones, M. R.; Van Mourik, F.; Van Stokkum, I. H. M.; Van Grondelle, R. *Biochemistry* **1997**, *36*, 6855−6861.

(24) Vos, M. H.; Breton, J.; Martin, J.-L. *J. Phys. Chem. B* **1997**, *101*, 9820−9832.

(25) Van Brederode, M. E.; Jones, M. R.; Van Grondelle, R. *Chem. Phys. Lett.* **1997**, *268*, 143.
(26) Thompson, M. A.; Zerner, M. C. *J. Am. Chem. Soc.* **1991**, *113*, 8210.
(27) Parson, W. W.; Warshel, A. *J. Am. Chem. Soc.* **1987**, *109*, 6152.
(28) Scherer, P. O. J.; Fischer, S. F. *Chem. Phys.* **1989**, *131*, 115−127.
(29) Won, Y.; Friesner, R. A. *J. Phys. Chem.* **1988**, *92*, 2208−2214.
(30) Won, Y.; Friesner, R. A. *J. Phys. Chem.* **1988**, *92*, 2215−2219.
(31) Friesner, R.; Won, Y. *Biochim. Biophys. Acta* **1989**, *77*, 99−122.
(32) Lathrop, E. J. P.; Friesner, R. A. *J. Phys. Chem.* **1994**, *98*, 3056−3066.
(33) Cho, M.; Yu, J.-Y.; Joo, T.; Nagasawa, Y.; Passino, S.; Fleming, G. R. *J. Phys. Chem.* **1996**, *100*, 11944−11953.
(34) Joo, T.; Jia, Y.; Yu, J.; Lang, M. J.; Fleming, G. R. *J. Chem. Phys.* **1996**, *104*, 6089−6108.
(35) De Boeij, W.; Psenichnikov, M. S.; Wiersma, D. A. *Chem. Phys. Lett.* **1996**, *253*, 53−60.
(36) Jiminez, R.; Van Mourik, F.; Fleming, G. R. *J. Phys. Chem. B* **1997**, *101*, 7350−7359.
(37) Yu, J.-Y.; Nagasawa, Y.; Van Grondelle, R.; Fleming, G. R. *Chem. Phys. Lett.* **1997**, *280*, 404−410.
(38) Homoelle, B. J.; Edington, M. D.; Diffey, W. M.; Beck, W. F. *J. Phys. Chem. B* **1998**, *102*, 3044−3052.
(39) Wraight, C. A. *Biochim. Biophys. Acta* **1979**, *548*, 309.
(40) Balk, M. W.; Fleming, G. R. *J. Chem. Phys.* **1985**, *83*, 4300−4307.
(41) Walmsley, I. A.; Mitsunaga, M.; Tang, C. L. *Phys. Rev. A* **1988**, *38*, 4681−4689.
(42) Cherepy, N. J.; Shreve, A. P.; Moore, L. J.; Boxer, S. G.; Mathies, R. A. *J. Phys. Chem. B* **1997**, *101*, 3250−3260.
(43) Nagasawa, Y.; Passino, S. A.; Joo, T.; Fleming, G. R. *J. Phys. Chem.* **1997**, *106*, 44840−44852.
(44) Nagasawa, Y.; Yu, J.-Y.; Fleming, G. R. *J. Chem. Phys.*, submitted.
(45) Kirmaier, C.; Holten, D.; Parson, W. W. *Biochim. Biophys. Acta* **1985**, *810*, 49−61.
(46) Mukamel, S. *Principles of Nonlinear Optical Spectroscopy*; Oxford University Press: New York, 1995; Chapter 8.
(47) Breton, J. In *The Photosynthetic Bacterial Reaction Center-Structure and Dynamics*; Breton, J., Vermeglio, A., Eds.; Plenum: New York, 1988; Vol. 149; pp 59−69.
(48) Mukamel, S. *Chem. Phys. Lett.* **1995**, *242*, 17−26.
(49) Jean, J. M.; Fleming, G. R. *J. Phys. Chem.* **1995**, *99*, 2092−2101.
(50) Scholes, G. D.; Harcourt, R. D.; Fleming, G. R. *J. Phys. Chem. B* **1997,** *101*, 7302−7312.
(51) Förster, T. In *Modern Quantum Chemistry*; Sinanoglu, O., Ed.; Academic Press: New York, 1965; Vol. III, pp 93−137.
(52) Lyle, P. A.; Kolaczkowski, S. V.; Small, G. J. *J. Phys. Chem.* **1993**, *97*, 6924−6933.
(53) Raja, N.; Reddy, S.; Kolaczkowski, S. V.; Small, G. J. *J. Phys. Chem.* **1993**, *97*, 6934−6940.
(54) Vos, M. H.; Jones, M. R.; Hunter, C. N.; Breton, J.; Lambry, J.-C.; Martin, J.-L. *Biochemistry* **1994**, *33*, 6750−6757.
(55) Vos, M. H.; Rappaport, F.; Lambry, J.-C.; Breton, J.; Martin, J.-L. *Nature* **1993**, *363*, 320−325.
(56) Shreve, A. P.; Cherepy, N. J.; Franzen, S.; Boxer, S. G. *Proc. Natl. Acad. Sci. U.S.A.* **1991**, *88*, 11207−11211.
(57) Alden, R. G.; Parson, W. W.; Chu, Z. T.; Warshel, A. *J. Phys. Chem.* **1996**, *100*, 16761−16770.
(58) Gehlen, J. N.; March, M.; Chandler, D. *Science* **1994**, *263*, 499−502.
(59) Woodbury, N. W. T.; Parson, W. W. *Biophys. Biochim. Acta* **1984**, *767*, 345−361.
(60) Peloquin, J. M.; Williams, A. C.; Lin, X.; Alden, R. G.; Taguchi, A. K. W.; Allen, J. P.; Woodbury, N. W. *Biochemistry* **1994**, *33*, 8089−8100.
(61) Agarwal, R.; Xu, Q.; Fleming, G. R. Work in progress.